October 7 Terror Attack: A One-Day Case Series of Imaging Trauma Patients at a Single Medical Center

Dana Brin MD[1,3], Vera Sorin MD[1,3], Noam Tau MD[1,3], Matan Kraus MD[1,3], Tom Sonin MD[1,3], Yiftach Barash MD[1,3], Evgeni Druskin MD[1], Eyal Klang MD[1,3], Christine Dan-Lantsman MD[1,3], Daniel Raskin MD[1,3], Elena Bekker MD[1,3], Shai Shrot MD[1,3], Amit Gutkind PhD[2], Olga Saukhat MD[1,3], Edith M. Marom MD[1,3], and Michal M. Amitai MD[1,3]

[1]Department of Diagnostic Imaging, Sheba Medical Center, Tel Hashomer, Israel
[2]Quality and Safety of Care unit, Sheba Medical Center, Tel Hashomer, Israel
[3]Faculty of Medicine, Tel Aviv University, Tel Aviv, Israel

ABSTRACT In this study, we analyzed computed tomography (CT) radiological findings from trauma treated at a single hospital in the aftermath of the terror attack in Israel on 7 October 2023. The study includes images from 34 consecutive patients, consisting of 33 males and 1 female, ranging in age from 19 to 68 years. The majority of these patients underwent both chest-abdominal-pelvic (76%) and head and neck CT scans (64.7%). Key findings highlight a high incidence of head and neck injuries (55.9%), chest trauma (44.1%), and various injuries such as soft tissue lacerations (100%), fractures (58.8%, particularly skull fractures [32.4%]), and brain hemorrhages (23.5%). The limitations of this study include its single-center scope and the focus on stable patients, which may bias the representation of injury types. This case series provides critical insights into the radiological impacts of large-scale terror events, emphasizing the importance of comprehensive preparedness and research in the field of mass-casualty incident response.

IMAJ 2023; 25: 780–786

KEY WORDS: diagnostic imaging, penetrating head injuries, soft tissue injuries, thoracic injuries, war-related injuries

On 7 October 2023, Israel experienced a devastating terror attack, which resulted in a huge number of trauma patients who were referred to multiple medical centers. In this study, we examined the radiological computed tomography (CT) findings of patients treated at our hospital on that day.

MATERIALS AND METHODS

This study was conducted at the Sheba Medical Center, a large Israeli tertiary facility. A retrospective review was performed of all trauma CT scans performed on 7 October 2023 as recorded in the radiology information system (RIS) of our hospital. We included all trauma CT scans of patients injured in the terror attack on 7 October who arrived at our medical facility on that day.

Patient records and radiological reports were reviewed for patient age, sex, CT scan type, and radiological findings. Data were anonymized and collected in compliance with ethics standards. This study was approved by our institutional review board (IRB 0825-23-SMC-D).

RESULTS

A total of 34 patients were included in this study, which was comprised of 33 males and 1 female. Their ages ranged from 19 to 68 years with a mean age of 31 years. The majority (76%) underwent chest-abdominal-pelvic CT scans. In addition, 64.7% needed head and neck CT scans, and 32.4% required CT scans of the upper or lower extremities. Detailed results are presented in Table 1.

Table 1. Trauma patient demographics (N=34)

Characteristic	n (%)
Age in years	
Mean	31.3
Range	19–68
Sex	
Male	33 (97.1)
Female	1 (2.9)
Computed tomography scan*	
Head and neck	22 (64.7)
Chest-abdomen-pelvis	26 (76.5)
Upper/lower extremities	11 (32.4)

*Patients may have presented with more than one injury

As shown in Table 2, the most common anatomical site of injury was the head and neck (55.9%) [Figures 1-8], followed by the chest (44.1%) [Figures 7-10], upper extremity (38.2%) [Figure 11], abdomen and pelvis (26.5%) [Figures 8C and 13], and lower extremity (20.6%) [Figure 12].

Table 2. Anatomical distribution of trauma injuries findings (N=34)

Anatomical zone	n (%)*
Head and neck	19 (55.9)
Chest	15 (44.1)
Abdomen and pelvis	9 (26.5)
Upper extremities	13 (38.2)
Lower extremities	7 (20.6)

*Patients may have presented with more than one injury

Figure 1. 21-year-old male. Coronal **[A]** and axial **[B]** non-contrast head CT images showing a penetrating injury in the vertex (white arrow) with multiple radiodense shrapnel in the brain parenchyma (black arrows)

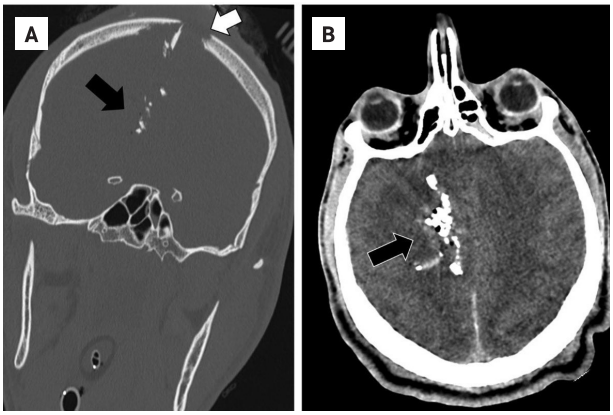

Figure 2. 30-year-old male. Lateral scout image of the head showing multiple extra-cranial shrapnel (white arrowheads) **[A]**; axial non-contrast head CT demonstrating right parietal bone fracture (black arrow), sub-arachnoid hemorrhage (black arrowheads) and an extra-axial bullet fragment (white arrow) **[B, C]**

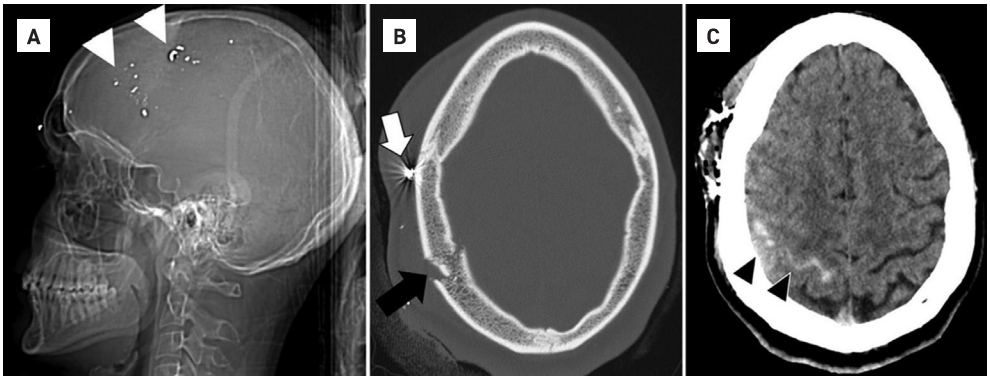

Figure 3. 46-year-old male. Scout **[A]**, coronal **[B]**, and axial **[C]** head CT images of a penetrating injury with comminuted frontal fractures (white arrow) and multiple bullet fragments (white arrowheads) accompanied by frontal contusions

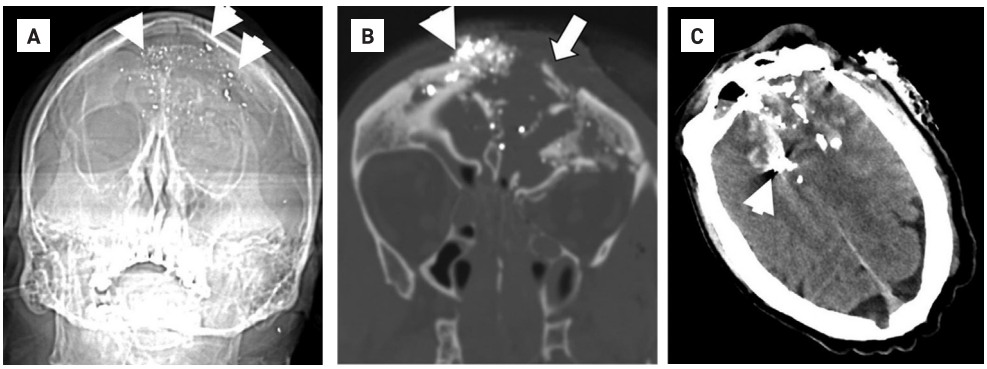

Figure 4. 42-year-old male. Comminuted mandible fracture (white arrows) shown in 3-dimensional reconstruction **[A]** and axial head CT images **[B]**

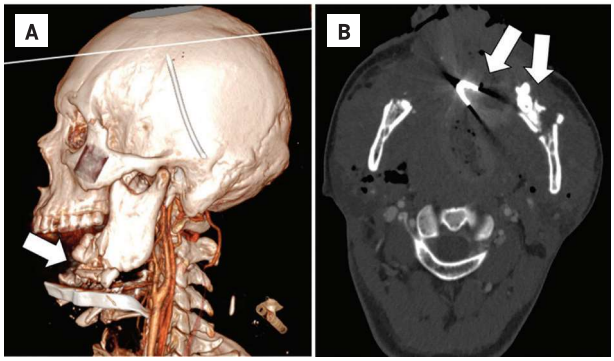

Figure 5. 32-year-old male. Axial bone CT image with multiple fractures of the walls of the maxillary sinuses (white arrows) that are filled with blood

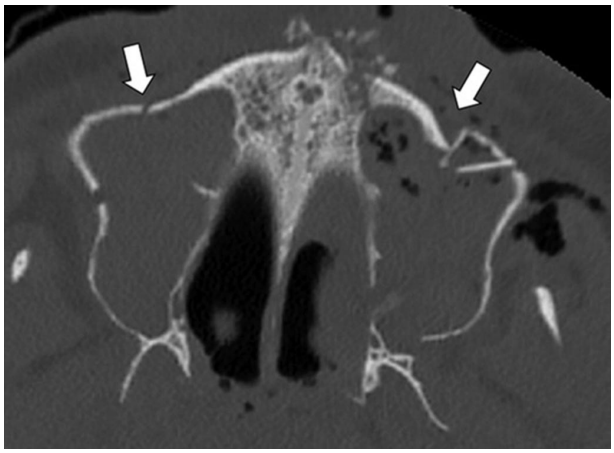

Figure 6. 19-year-old male. Axial head CT image with comminuted mandibular fracture (white arrow)

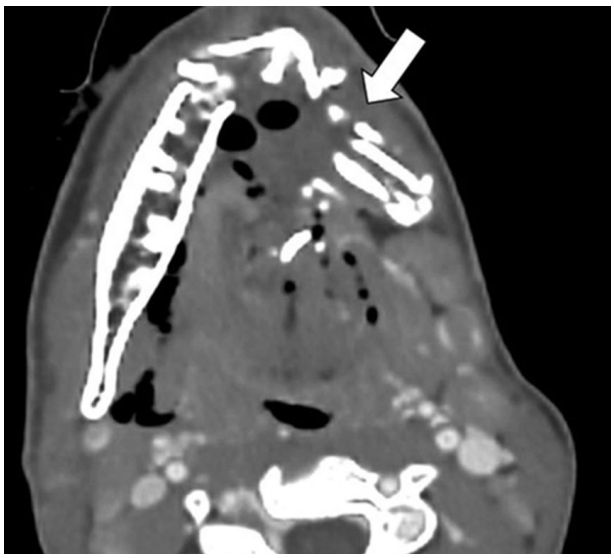

Figure 7. 21-year-old male. Scout image of the head **[A]** and axial non-contrast head CT **[B]** with a midline bullet fragment (white arrow) within the brain parenchyma. Left globe rupture can also be seen (white arrowhead). Axial contrast-enhanced chest CT **[C]** showing a penetrating injury in the left chest wall (white arrow) with pneumothorax (white arrowhead) and left lung contusion (black arrow)

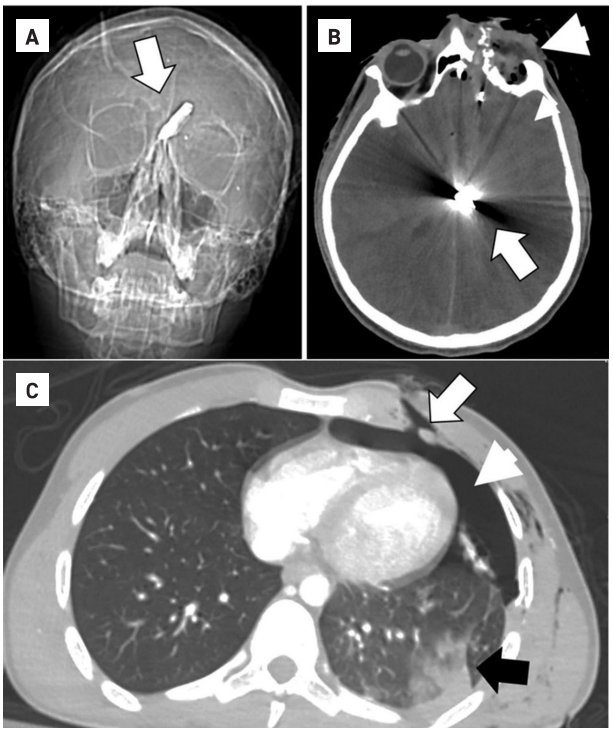

The variety of injury types is detailed in Table 3. All patients included in this study presented with soft tissue lacerations due to bullet fragments. In addition, 58.8% showed evidence of bone fractures, most commonly in the skull (32.4%) [Figures 7C, 8B, 9, 10], Brain hemorrhaging occurred in 23.5% of patients [Figure 2C].

Chest injuries included lung contusions and lacerations (26.5%) [Figures 7C, 8, 9, 10], pneumothorax (14.7%) [Figures 7C ,8B, 9C], hemothorax (8.8%), and pneumomediastinum (2.9%). Three patients (8.8%) presented with pneumoperitoneum [Figure 8C], suggestive of bowel injury. Three patients (8.8%) sustained parenchymal organ injuries [Figure 8C]. Vascular injuries were found in four patients (11.8%) [Figure 13].

DISCUSSION

This case series offers a comprehensive analysis of the radiological findings from a single medical center following the catastrophic terror attack on 7 October 2023

Figure 8. 23-year-old female. Axial non-contrast head CT showing a bullet fragment in the brain parenchyma (white arrow). The bullet penetrated through the eye globe (white arrowhead) and the brain parenchyma **[A]**; axial chest CT contrast-enhanced showing a large right pneumothorax (black arrowheads), mediastinal shift to the left despite the presence of a chest drainage (white arrowhead) **[B]**; axial abdominal contrast-enhanced CT demonstrating right renal contusion (white arrow) and pneumoperitoneum (white arrowheads) **[C]**

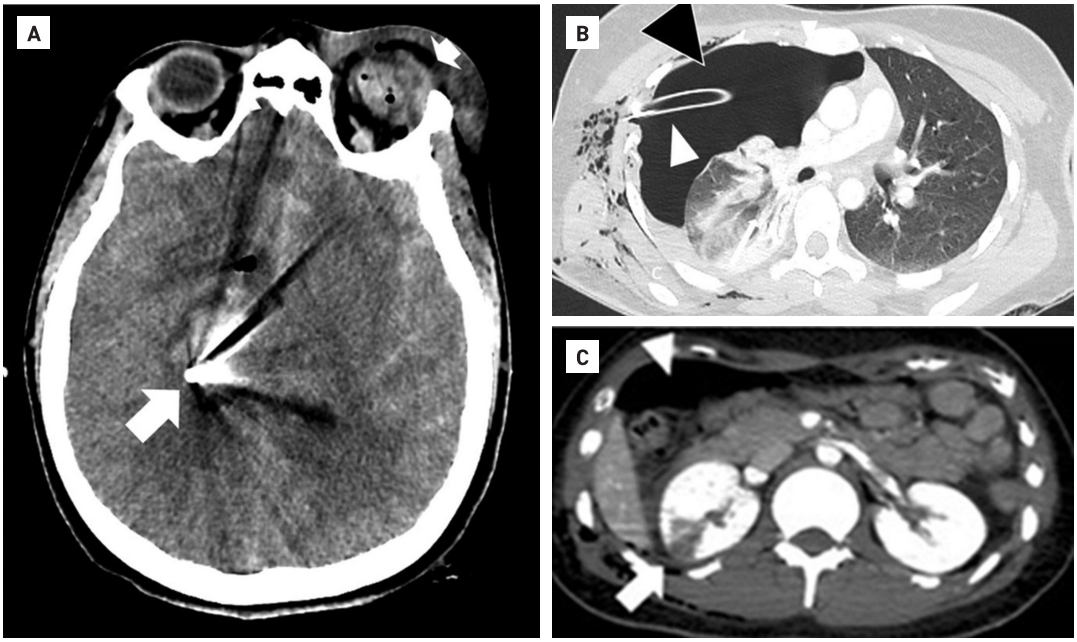

Figure 9. 19-year-old male. A scout image **[A]**, coronal **[B]**, and axial **[C]** contrast-enhanced chest CT images of a penetrating trauma with right chest wall subcutaneous emphysema (black arrow), lung contusion (white arrows), and pneumothorax (black arrowhead)

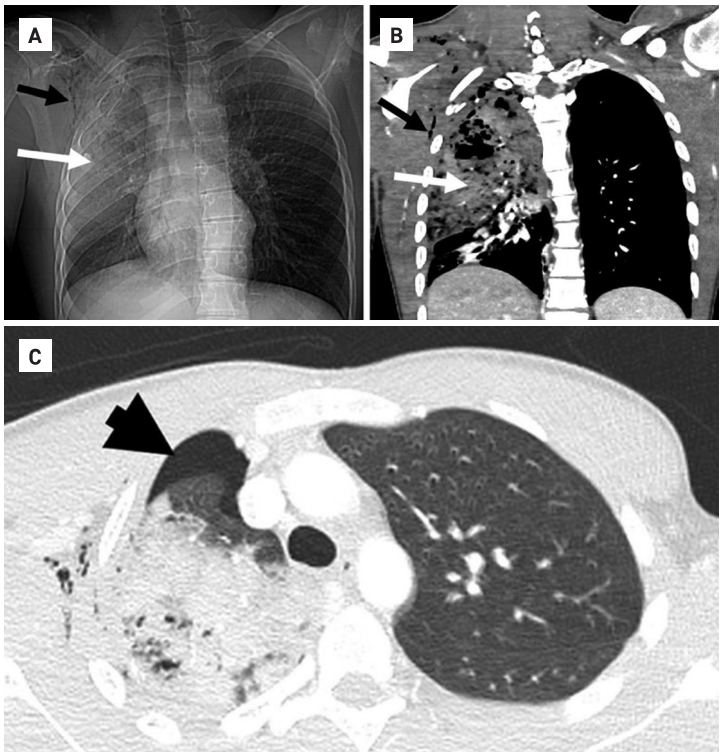

Figure 10. 49-year-old male. Scout **[A]**, coronal **[B]**, and axial **[C]** contrast-enhanced chest CT images of a penetrating trauma to the left chest wall and lung. There are multiple bullet fragments in the soft tissues (white arrowheads), posterior rib and scapula fractures (white arrows), and left lung contusion (black arrow)

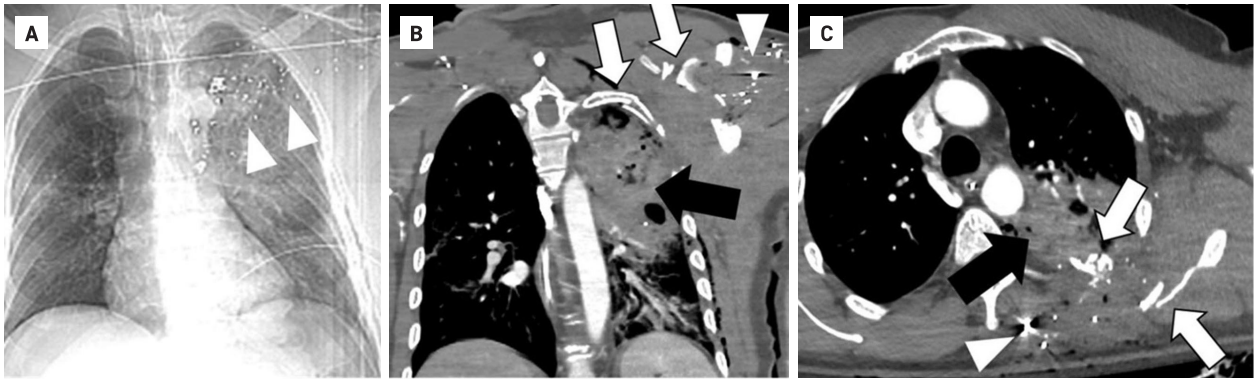

in Israel. The study, focusing on CT scan results, shows the extent and severity of the injuries.

Our results align with the expected consequences of ballistic trauma, including injuries from high-velocity gunshot wounds and grenade explosions [1–3]. All patients included in this review showed evidence of soft tissue lacerations and hematomas, typical in an attack of this nature. The most common injury locations were the head and neck (55.9%), followed by chest injuries (44.1%), which included lung contusions (26.5%), pneumothorax (14.7%), and chest wall fractures (20.6%). Skull fractures (32.4%) and injuries to the extremities (23.5%) were also prevalent.

This study has several limitations. As a medical center located more than 70 kilometers from the epicenter of the attack, our hospital did not experience the initial influx of emergency cases. This geographical factor likely influenced the number and types of injuries we encountered. Furthermore, we only included patients who presented to our center on 7 October. Subsequent arrivals, both direct and via transfer, were not covered in this analysis but may provide further insights into the evolving nature of the injuries and medical responses.

In addition, our study reflects a selection bias toward stable patients. Unstable patients who required immediate surgical or angiographic embolization interventions and those who only underwent X-ray imaging or ultrasound were excluded from our radiological review.

Table 3. Trauma injuries findings (N=34)

Injury type	n (%)*
Soft tissue	**34 (100)**
Fractures	**20 (58.8)**
Skull	11 (32.4)
Chest wall	7 (20.6)
Pelvis	2 (5.9)
Upper extremity	5 (14.7)
Lower extremity	3 (8.8)
Vascular injury	**4 (11.8)**
Brain hemorrhage	**8 (23.5)**
Chest injuries	**15 (44.1)**
Lung contusion / laceration	9 (26.5)
Pneumothorax	5 (14.7)
Hemothorax	3 (8.8)
Pneumomediastinum	1 (2.9)
Parenchymal organ contusion / laceration	**3 (8.8)**
Liver	1 (2.9)
Spleen	1 (2.9)
Kidney	1 (2.9)
Adrenal	1 (2.9)
Pneumoperitoneum	**3 (8.8)**

*Patients may have presented with more than one injury

CONCLUSIONS

In this case series, we provided initial insights into the radiological aspects of trauma management following a large-scale terror event. We highlighted the complexities and limitations inherent in medical research post-catastrophe. These findings offer a glimpse into the nature of injuries sustained and emphasize the need for ongoing research and preparedness for future mass-casualty events.

Figure 11. 21-year-old male. Pelvic scout image with multiple bullet fragments in both hands (black arrows)

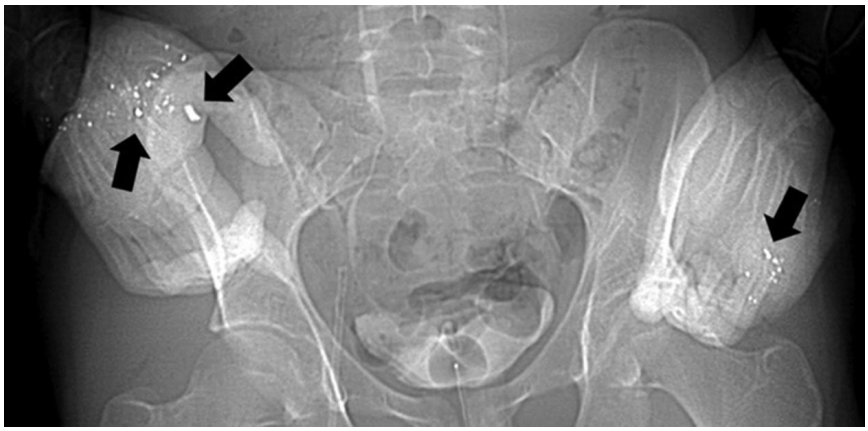

Figure 12. 26-year-old male. Axial CT of the lower extremities with left medial thigh hematoma (white arrow) surrounding a bullet fragment (white arrowhead)

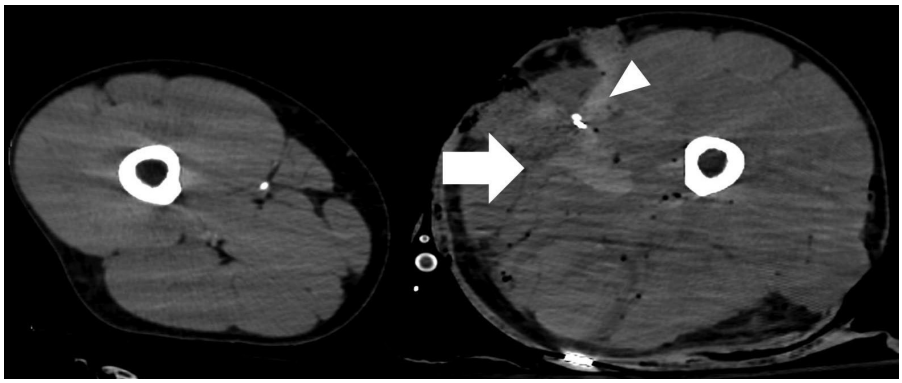

Figure 13. 36-year-old male. Axial pelvic CT **[A]** showing explosion fragments (white arrow) causing active arterial bleeding in the left buttock (white arrowhead); interventional angiography images of the active bleed **[B]** and post-embolization **[C]**

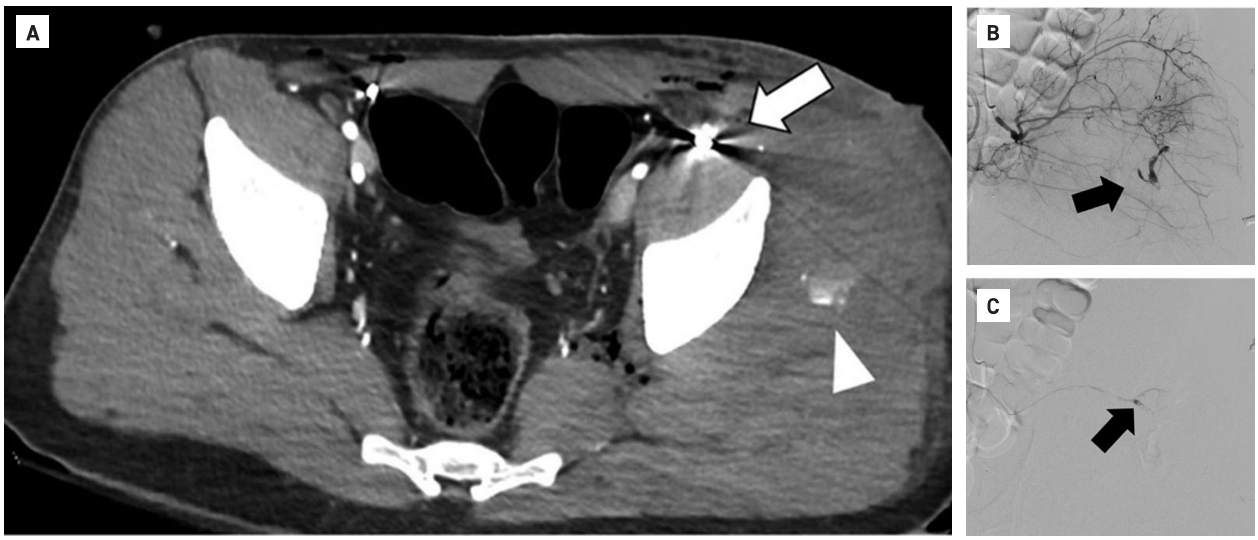

Acknowledgments

The authors thank the radiologists and radiology technicians from the Department of Diagnostic Imaging at Sheba Medical Center who assisted during this challenging day. In addition, the authors thank David Elisha for his contributions to the manuscript.

Correspondence

Dr. M.M. Amitai

Dept. of Diagnostic Imaging, Sheba Medical Center, Tel Hashomer 52621, Israel

Phone: (972-3) 530-2530

Fax: (972-3) 535-7315

Email: michal.amitai@sheba.health.gov.il

References

1. Benjaminov O, Sklair-Levy M, Rivkind A, Cohen M, Bar-Tal G, Stein M. Role of radiology in evaluation of terror attack victims. *AJR Am J Roentgenol* 2006; 187 (3): 609-16.
2. Naeem M, Hoegger MJ, Petraglia FW 3rd, et al. CT of penetrating abdominopelvic trauma. *Radiographics* 2021; 41 (4): 1064-81.
3. Durso AM, Paes FM, Caban K, et al. Evaluation of penetrating abdominal and pelvic trauma. *Eur J Radiol* 2020; 130: 109187.

Capsule

Deconstruction of rheumatoid arthritis synovium defines inflammatory subtypes

Rheumatoid arthritis is a prototypical autoimmune disease that causes joint inflammation and destruction. There is currently no cure for rheumatoid arthritis, and the effectiveness of treatments varies across patients, suggesting an undefined pathogenic diversity. To deconstruct the cell states and pathways that characterize this pathogenic heterogeneity, **Zhang** et al. profiled the full spectrum of cells in inflamed synovium from patients with rheumatoid arthritis. The authors used multi-modal single-cell RNA-sequencing and surface protein data coupled with histology of synovial tissue from 79 donors to build single-cell atlas of rheumatoid arthritis synovial tissue that includes more than 314,000 cells. They stratified tissues into six groups, referred to as cell-type abundance phenotypes (CTAPs), each characterized by selectively enriched cell states. These CTAPs demonstrate the diversity of synovial inflammation in rheumatoid arthritis, ranging from samples enriched for T and B cells to those largely lacking lymphocytes. Disease-relevant cell states, cytokines, risk genes, histology, and serology metrics are associated with particular CTAPs. CTAPs are dynamic and can predict treatment response, highlighting the clinical utility of classifying rheumatoid arthritis synovial phenotypes. This comprehensive atlas and molecular, tissue-based stratification of rheumatoid arthritis synovial tissue reveal new insights into rheumatoid arthritis pathology and heterogeneity that could inform novel targeted treatments.

Nature 2023; 623: 616

Eitan Israeli

Capsule

A molnupiravir-associated mutational signature in global SARS-CoV-2 genomes

Molnupiravir, an antiviral medication widely used against severe acute respiratory syndrome coronavirus 2 (SARS-CoV-2), acts by inducing mutations in the virus genome during replication. Most random mutations are likely to be deleterious to the virus and many will be lethal; thus, molnupiravir-induced elevated mutation rates reduce viral load. However, if some patients treated with molnupiravir do not fully clear the SARS-CoV-2 infections, there could be the potential for onward transmission of molnupiravir-mutated viruses. **Sanderson** and co-authors showed that SARS-CoV-2 sequencing databases contain extensive evidence of molnupiravir mutagenesis. Using a systematic approach, the authors found that a specific class of long phylogenetic branches, distinguished by a high proportion of G-to-A and C-to-T mutations, are found almost exclusively in sequences from 2022, after the introduction of molnupiravir treatment, and in countries and age groups with widespread use of the drug. The authors identified a mutational spectrum, with preferred nucleotide contexts, from viruses in patients known to have been treated with molnupiravir and showed that its signature matches that seen in these long branches, in some cases with onward transmission of molnupiravir-derived lineages. Finally, they analyzed treatment records to confirm a direct association between these high G-to-A branches and the use of molnupiravir.

Nature 2023; 623: 594

Eitan Israeli